

Observation of superconductivity and anomalous electrical resistivity in single-crystal Ir₃Te₈L. Li,¹ T. F. Qi,¹ L. S. Lin,² X. X. Wu,³ X. T. Zhang,³ K. Butrouna,¹ V. S. Cao,^{1,*} Y. H. Zhang,² Jiangping Hu,^{3,4}
S. J. Yuan,^{1,5} P. Schlottmann,⁶ L. E. De Long,¹ and G. Cao^{1,†}¹*Department of Physics and Astronomy, Center for Advanced Materials, University of Kentucky, Lexington, Kentucky 40506, USA*²*High Magnetic Field Laboratory, Chinese Academy of Sciences, Hefei 230031, China*³*Beijing National Laboratory for Condensed Matter Physics, Institute of Physics, Chinese Academy of Sciences, Beijing, China*⁴*Department of Physics, Purdue University, West Lafayette, Indiana 47907, USA*⁵*Department of Physics, Shanghai University, Shanghai, China*⁶*Department of Physics, Florida State University, Tallahassee, Florida 32306, USA*

(Received 10 January 2013; revised manuscript received 26 April 2013; published 13 May 2013)

We observe an unusual combination of normal and superconducting state properties without any signature of strong spin fluctuations in single-crystal Ir₃Te₈. The electrical resistivity does not saturate by 700 K but exhibits a low-resistivity ratio, and it exhibits two extended linear regimes (approximately 20–330 and 370–700 K) with the same slope, separated by a small hysteretic interval marking a strong first-order phase transition from cubic to rhombohedral lattice symmetry at $T_S = 350$ K. The electronic heat-capacity coefficient ($11 \text{ mJ mol}^{-1} \text{ K}^{-2}$) is consistent with a net diamagnetic, rather than a Pauli paramagnetic, normal state that yields to superconductivity below a critical temperature $T_C = 1.8$ K. The size of the heat-capacity jump near T_C indicates bulk superconductivity.

DOI: [10.1103/PhysRevB.87.174510](https://doi.org/10.1103/PhysRevB.87.174510)

PACS number(s): 74.10.+v, 71.20.-b, 74.25.F-, 75.20.-g

I. INTRODUCTION

Ir compounds have recently emerged as a fertile ground for discoveries of new physics driven by large spin-orbit interactions (SOIs) typical of *5d* electronic states. The close competition among the SOIs, the crystalline electric fields, and the Coulomb interaction U stabilizes novel ground states and phenomena.^{1–6} These discoveries have stimulated a variety of theoretical predictions^{7–13} that await experimental confirmation, including topologically driven semimetallic¹² or superconducting¹³ states.

Herein, we report an unusual combination of phenomena in single-crystal Ir₃Te₈: The normal state is metallic, but the electrical resistivity does not exhibit the usual T^2 Fermi-liquid term. It does not saturate by 700 K and remains large ($\approx 0.46 \text{ m}\Omega \text{ cm}$) below 4 K. Moreover, Ir₃Te₈ is diamagnetic rather than Pauli paramagnetic,¹⁴ similar to nonsuperconducting Cu since the core diamagnetism of Ir and Te ions is larger than the Pauli susceptibility. Ir₃Te₈ superconducts below a critical temperature $T_C = 1.8$ K, presumably due to a substantial electron-phonon coupling. It is remarkable that the resistivity slope remains essentially unchanged through a first-order phase transition at $T_S = 350$ K, which separates a high-temperature cubic phase from a low-temperature rhombohedral phase; this implies that the carrier density and the electron-phonon coupling are not affected by the structural change. Most structural and physical properties reported here are unique to single-crystal Ir₃Te₈ and have not been observed in polycrystalline samples.^{14,15}

Superconductivity has recently been found in Ir-based chalcogenides, namely, CdI₂-type Ir_{1-x}M_xTe₂ ($M = \text{Pd}$ and Pt) (Refs. 16–19) and Ir_xSe₂ ($x > 0.75$) pyrites.²⁰ Superconducting Ir_{1-x}M_xTe₂ is a derivative of layered IrTe₂, which exhibits a structural transition near 260 K from a rhombohedral to a low-temperature monoclinic structure. This transition was attributed to a possible charge-density wave (CDW),¹⁶ although no CDW gap has yet been detected.^{18,19}

Nevertheless, superconducting transitions with T_C as high as 3 K emerge with the suppression of the structural transition in doped Ir_{1-x}M_xTe₂,¹⁶ similar to classic CDW compounds, such as NbSe₂ and (Nb_{1-x}Ta_x)Se₃.^{20,21} Higher T_C 's of up to 6.4 K were found in a polycrystalline Ir_{0.91}Se₂ pyrite,¹⁵ which is a nonstoichiometric variant of a parent Ir_{0.75}Se₂ (or Ir₃Se₈) compound of rhombohedral space group $R\bar{3}$ and is proximate to a metal-insulator transition. We note that no high-temperature phase transitions similar to that found in layered IrTe₂ are reported for relatively high- T_C Ir_xSe₂ compositions.¹⁵ Superconductivity in these Ir-based chalcogenides is evidently not as sensitive to crystal structure as it is for many other transition-metal materials for which narrow peaks in the electronic density of states promote T_C 's that range from 10 to 20 K.²² Moreover, these chalcogenides sharply contrast with known Ir oxides where a strong SOI generally drives narrow-gap insulating states.^{1,2,23–27}

II. EXPERIMENT

Single crystals of Ir₃Te₈ were grown by a slow-cooling technique using excess Te as the flux. Stoichiometric quantities of the elements were ground thoroughly and were sealed in an evacuated quartz tube, which was slowly heated up to 1000 °C and was held at that temperature for 7 days. The synthesized polycrystalline Ir₃Te₈ was then mixed with an appropriate amount of Te powder and was sealed under vacuum in a small quartz tube, which was, subsequently, set in a larger quartz tube that was then evacuated and was sealed. The mixture was heated up to 1050 °C where it was maintained for over 48 h, followed by slow cooling to 700 °C. The average size of the single crystals was $1 \times 1 \times 1 \text{ mm}^3$ as shown in Fig. 1. Measurements of magnetization $M(T, H)$, heat capacity $C(T)$, and electrical resistivity $\rho(T)$ were performed over the temperature interval of $0.5 \text{ K} < T < 700 \text{ K}$ using either a Quantum Design (QD) physical property measurement system

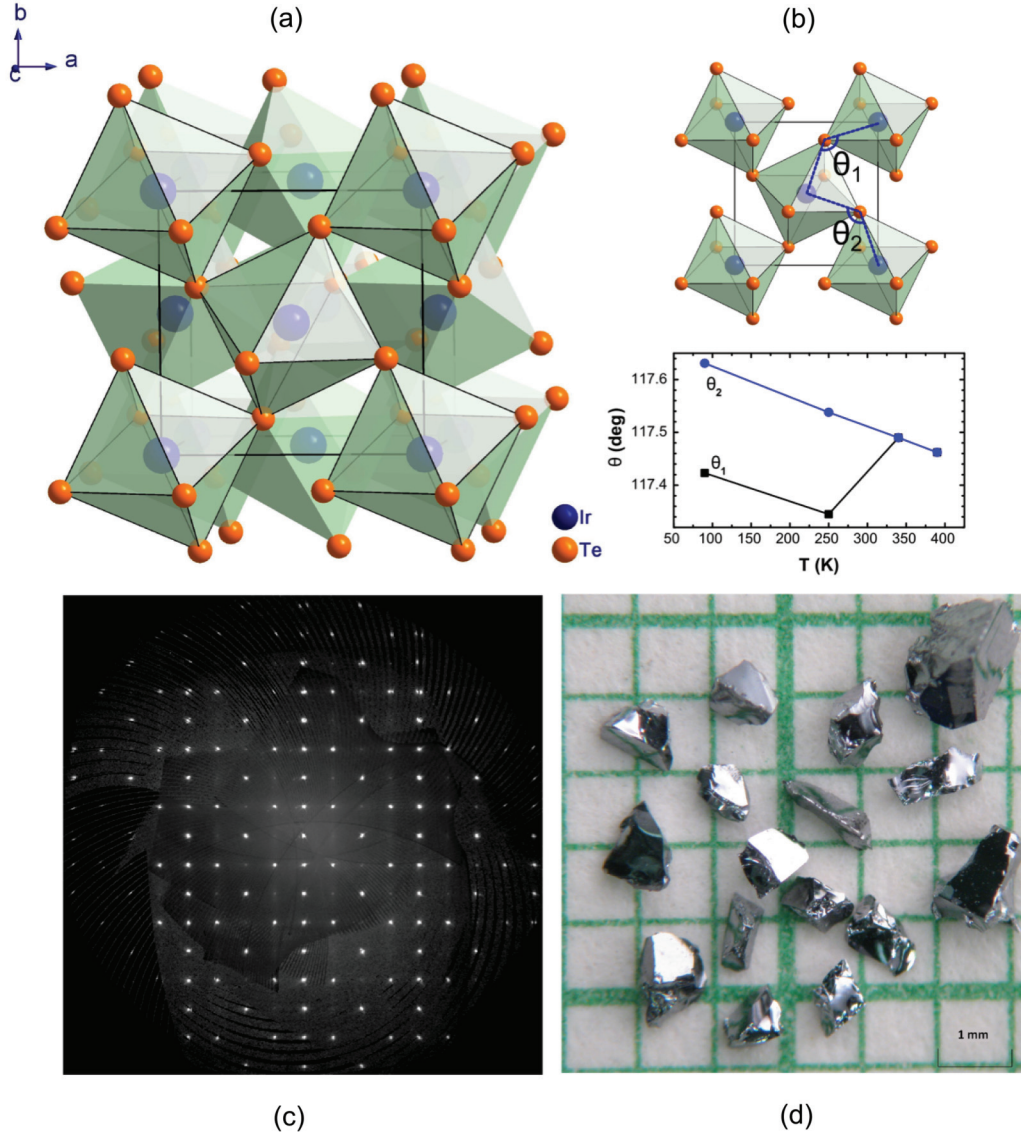


FIG. 1. (Color online) (a) The crystal structure of Ir_3Te_8 , (b) the definition of the bond angles θ_1 and θ_2 (upper panel) and the temperature dependence of θ_1 and θ_2 (lower panel), (c) a representative x-ray diffraction pattern at $T = 295$ K for $[h\ 1\ l]$, and (d) representative single crystals of Ir_3Te_8 .

or a QD magnetic property measurement system equipped with a Linear Research Model LR-700 ac bridge. The high temperature $\rho(T)$ was measured using a Displex closed-cycle cryostat capable of continuous temperature ramping from 9 to 900 K.

III. BAND-STRUCTURE CALCULATION

Density functional theory calculations were carried out using the projector augmented wave method encoded in the Vienna *ab initio* simulation package^{28–30} and employed the generalized-gradient approximation for the exchange-correlation functional.³¹ The SOIs of the valence electrons were included using the second-variation method for the scalar-relativistic eigenfunctions of the valence states.³² The plane-wave basis set cutoff was set at 500 eV. The Brillouin zone was sampled using the Monkhorst-Pack scheme³³ with $(7 \times 7 \times 7)$ \mathbf{k} points for the Ir_3Te_8 and Ir_4Te_8 primitive

cells. The lattice parameters used were $a = 6.4024$ Å and $\alpha = 90.017^\circ$ (measured at 90 K, see Table I). The atomic positions were fully relaxed, and forces were minimized to less than 0.01 eV/Å.

IV. RESULTS AND DISCUSSION

The crystal structure of a small single crystal was determined using Mo $K\alpha$ radiation and a Nonius Kappa CCD

TABLE I. Lattice parameters for Ir_3Te_8 .

Temperature (K)	90	250	390
a (Å)	6.4024	6.4081	6.4152
α (deg)	90.017	90.017	90
Structure	Rhombohedral	Rhombohedral	Cubic
(Space group)	($R-3$)	($R-3$)	($Pa3$)

single-crystal diffractometer at temperatures of $T = 90, 250, 295, 350$, and 390 K. The structures were refined using the SHELX-97 programs.^{34,35} Crystal composition was examined by energy-dispersive x-ray spectroscopy using a Hitachi/Oxford SwiftED 3000. The R and R_w factors are low, 0.025 and 0.058, respectively, and the mosaicity was also small, suggesting well-ordered crystals, as shown in Figs. 1(c) and 1(d). The Ir site occupancy was freely varied and was found to be 80%. A superlattice was evident in all x-ray diffraction data, suggesting the Ir vacancies order in our crystals [see Fig. 1(b)]. Given the possible existence of inhomogeneities in these materials,¹⁷ the structural and physical properties of a number of Ir_3Te_8 crystals were examined, and we found no discernible discrepancies between data for all measured crystals. The 80% occupation of the Ir sites gives rise to disorder scattering of the conduction electrons and is a likely explanation for the large residual resistivity.

The room-temperature crystal structure of Ir_3Te_8 was initially reported to be cubic with space group $Pa\bar{3}$ (Ref. 36) but was, subsequently, described as rhombohedral with space group $R\bar{3}$.³⁷ Our single-crystal x-ray refinements show Ir_3Te_8 undergoes a structural phase transition near $T_S = 350$ K, changing from a high-temperature cubic lattice with space group $Pa\bar{3}$ (No. 205) to a low-temperature rhombohedral lattice with space group $R\bar{3}$ (No. 148) (see Table I). The difference between the two structures can be defined by the difference $\Delta\theta$ ($\equiv\theta_1 - \theta_2$) between two bond angles θ_1 ($\text{Ir}_1\text{-Te}_1\text{-Ir}_2$) and θ_2 ($\text{Ir}_2\text{-Te}_2\text{-Ir}_1$); i.e., $\Delta\theta$ is zero for $T \geq T_S = 350$ K when the lattice is cubic and finite for $T < T_S$ where the lattice symmetry is reduced to rhombohedral [see Figs. 1(a) and 1(b)]. The structural transition is subtle but, nevertheless, causes strong anomalies in the transport and magnetic properties as discussed below.

Our heat-capacity data $C(T)$ for $50 \text{ mK} \leq T < 300$ K yield a Debye temperature of $\theta_D = 246$ K and an electronic coefficient $\gamma = 11 \text{ mJ mol}^{-1} \text{ K}^{-2}$. These values are quite similar to those for Ir_xSe_2 .¹⁵ Single-crystal Ir_3Te_8 is distinctly metallic (although highly resistive) throughout a wide temperature range [see Fig. 2(a)], which sharply contrasts the insulating behavior of Ir_3Se_8 .¹⁵ The a -axis electrical resistivity $\rho_a(T)$ is interrupted by a strong first-order anomaly with hysteresis in the vicinity of $T_S = 350$ K, which is consistent with the lattice transition revealed in the structural data. Except for $T < 20$ K (including an onset of superconductivity at $T_C = 1.8$ K) and the vicinity of T_S , the slope of $\rho_a(T)$ remains unchanged over a remarkably wide temperature range of $20 \text{ K} \leq T \leq 700$ K, in particular, both below and above T_S .

An extended regime of linear- T resistivity is a classic signature of high- T_C cuprates and the p -wave superconductor Sr_2RuO_4 , Fe-based superconductors, and many other correlated oxides³⁸ in which spin fluctuations play an important role in the electron scattering. In contrast, Ir_3Te_8 is diamagnetic (see below), and the application of high magnetic fields up to 14 T causes no changes near the anomaly at T_S or $\rho_a(T)$ at $T \gg T_C$ (not shown). These observations confirm that the observed behavior in $\rho_a(T)$ for Ir_3Te_8 must have an origin other than spin scattering. Elementary Bloch-Grüneisen theory predicts $\rho(T) \sim T^5$ for $T < (0.2)\theta_D \sim 49$ K (we find the Debye temperature of $\theta_D = 246$ K for Ir_3Te_8), and $\rho(T) \sim T$ for $T \gg \theta_D$, in the case of electron-phonon scattering. The linearity of resistivity

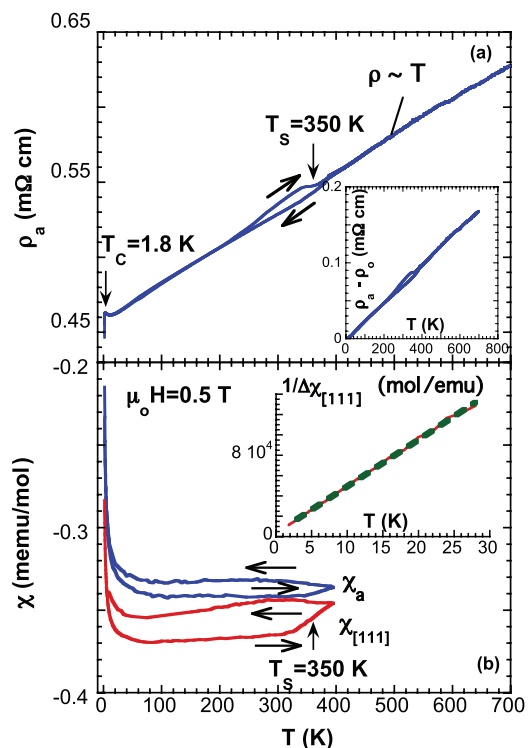


FIG. 2. (Color online) (a) The temperature dependence of the a -axis resistivity $\rho_a(T)$ for $1.7 \text{ K} \leq T \leq 700 \text{ K}$. Inset: $[\rho_a(T) - \rho_0]$ as a function of temperature for $10 \text{ K} \leq T \leq 700 \text{ K}$. (b) The temperature dependence of the magnetic susceptibility $\chi_{[111]}(T)$ along the direction $[111]$ and $\chi_a(T)$ along the a axis at $\mu_0 H = 0.5 \text{ T}$ for $1.7 \text{ K} \leq T \leq 395 \text{ K}$. Inset: $(\Delta\chi)^{-1}_{[111]}$ vs T for $1.7 \text{ K} \leq T \leq 30 \text{ K}$ where $\Delta\chi_{[111]} \equiv \chi_{[111]} - \chi_0$ and $\chi_0 = -0.000372 \text{ emu/mol}$.

in an extended regime is seen for some elements, such as copper and platinum. However, only a handful of materials exhibit an extended regime of linear- T resistivity that accompanies superconductivity; indeed, “resistivity saturation” is anticipated when the mean-free path l of the quasiparticles becomes shorter than the lattice parameter a (Mott-Ioffe-Regel limit^{39,40}) or for $\rho \sim 100\text{--}150 \mu\Omega \text{ cm}$ (Mooij limit^{41,42}). The experimental values of $\rho_a(T)$ for Ir_3Te_8 are well above the Mott-Ioffe-Regel or Mooij limits, yet $\rho_a(T)$ shows no sign of saturation up to 700 K. What is intriguing is that $\rho_a(T)$ shows no slope change near T_S , despite the fact that the first-order structural change that must affect the electronic state. At low temperatures, $\rho_a(T)$ shows a Kondo-like minimum near 20 K without the usual T^2 Fermi-liquid term, but it remains large (the residual resistivity of $\rho_0 \approx 0.46 \text{ m}\Omega \text{ cm}$) between T_C and 10 K [Fig. 2(a)]. It deserves pointing out that, despite the large residual resistivity, the overall change in $\rho_a(T)$ between 10 and 700 K or $\rho_a(T) - \rho_0$ is on the order of $180 \mu\Omega \text{ cm}$ [see the Fig. 2(a) inset], which is quite reasonable for a low-density-of-states material ($\gamma = 11 \text{ mJ/mol Ir K}^2$), and consistent with both T_C and our specific heat jump data discussed below. This also shows that the overall change in resistivity is sufficient to clearly define a temperature power law of the high-temperature resistivity.

The magnetic susceptibility $\chi(T)$ of Ir_3Te_8 up to room temperature has been reported previously.¹⁴ The susceptibility for single crystals is anisotropic; remarkably, $\chi_{[111]}$ is more

diamagnetic than χ_a , and both exhibit a first-order anomaly in the vicinity of T_S as shown in Fig. 2(b). An unusually strong thermal hysteresis is seen in Fig. 2(b), consistent with a structural transition. Both $\chi_{[111]}(T)$ and $\chi_a(T)$ rapidly rise below 30 K; a Curie-Weiss fit of $\chi_{[111]}$ (warming portion) for $T < 30$ K yields a Curie-Weiss temperature of $\theta_{CW} = -0.7$ K and a small effective moment $\mu_{\text{eff}} = 0.024\mu_B/\text{Ir}$. Both the low-temperature susceptibility and the minimum in $\rho_a(T)$ near 12 K suggest a small concentration of impurity spins is present [see the inset in Fig. 2(b)]. Note that these impurity spins could be Ir ions with incomplete bonding. The net diamagnetic moment may not be entirely surprising, given the small value of the Sommerfeld heat-capacity coefficient $\gamma \approx 11 \text{ mJ mol}^{-1} \text{ K}^{-2}$, i.e., per three Ir ions, which is only slightly larger and comparable to that for diamagnetic Cu. The diamagnetism is due to the fact that both Ir and Te are heavy elements, and they have large core diamagnetism ($\chi_d(\text{Te}) = -7 \times 10^{-5} \text{ emu/mol}$ and $\chi_d(\text{Ir}) = -3.5 \times 10^{-5} \text{ emu/mol}$ ³⁷) that exceeds the Pauli paramagnetism. The net core diamagnetism is estimated to be $-6.7 \times 10^{-4} \text{ emu/mol}$ for Ir_3Te_8 , which is consistent with the experimental value of $-3.5 \times 10^{-4} \text{ emu/mol}$, considering that there must be a compensating contribution from the Pauli paramagnetism. It is noted that this scenario offers no clear explanation for the significant anisotropy of $\chi(T)$ illustrated in Fig. 2(b), which has to arise from the paramagnetic term, e.g., due to Van Vleck band contributions that reflect anisotropies of the electronic structure and/or small gaps between bands near the Fermi level (see below).

The transition of Ir_3Te_8 to superconductivity is shown in Fig. 3 where both $\rho_a(T)$ and $\chi_a(T)$ exhibit onsets at $T_C = 1.8$ K. $\rho_a(T)$ drops by 1 order of magnitude from $T_C = 1.80$ to 1.2 K but does not vanish at 1.2 K [$\rho_a(1.2 \text{ K}) = 4.5 \times 10^{-5} \Omega \text{ cm}$]. The relatively broad transition is unusual but consistent with the jump in the specific heat $C(T)$ and the weak short-range magnetic order evidenced in the data shown in Figs. 2 and 3. Indeed, application of a dc magnetic field H readily depresses T_C [see Fig. 3(a) inset] as expected. On the other hand, $\rho_a(T)$ exhibits a small positive magnetoresistive shift for $T > T_C$. If this would be due to short-range antiferromagnetic order or a Kondo-like effect, one would anticipate a negative magnetoresistance. Note that $\chi_a(T)$ exhibits little difference between zero-field-cooling and field-cooling measurements until the temperature decreases to 0.5 K as illustrated in Fig. 3(b). This indicates the superconducting state may not be fully established until well below 0.5 K. Nevertheless, an “equal-area” (entropy balancing) construction of the heat-capacity data near T_C (see Fig. 4) yields a conservative estimate of $\Delta C/\gamma T_C \approx 1.0$, which indicates bulk superconductivity; this estimate is also consistent with the partial suppression of the superconducting gap [corresponding to the fully gapped value $\Delta C/\gamma T_C \approx 1.43$ for the BCS model with $\gamma \approx 11 \text{ mJ mol}^{-1} \text{ f.u.}^{-1} \text{ K}^{-2}$ (where f.u. represents formula units)] by pair breaking due to magnetic impurities.⁴³ These scenarios are also consistent with estimates of an approximate 16% Meissner effect at 0.5 K when the demagnetization effect and flux pinning are taken into account. We conclude that a sizable superconducting volume exists in our crystal, even if the superconducting state is incompletely established over a substantial range of temperatures near T_C .

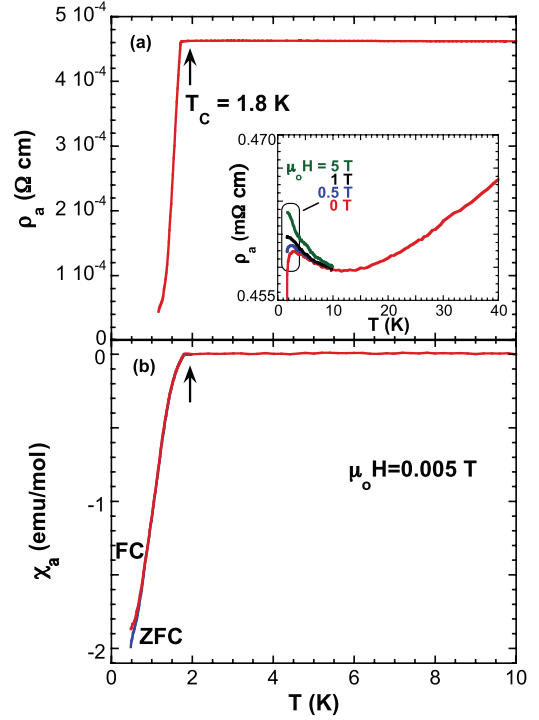


FIG. 3. (Color online) The temperature dependence of (a) the a -axis resistivity $\rho_a(T)$ for $1.0 \text{ K} \leq T \leq 10 \text{ K}$; and (b) the a -axis magnetic susceptibility $\chi_a(T)$ for $0.5 \text{ K} \leq T \leq 10 \text{ K}$ at $\mu_0 H = 0.005 \text{ T}$. Inset: The temperature dependence of $\rho_a(T)$ for $1.7 \text{ K} \leq T \leq 10 \text{ K}$ at $\mu_0 H = 0, 0.5, 1, \text{ and } 5 \text{ T}$.

Our electronic structure calculations for Ir_3Te_8 were performed by first carrying out a calculation for Ir_4Te_8 and then removing the Ir atoms located at the Wyckoff site a in a unit cell. Two bands derived from Ir- e_g and Te- $5p$ orbitals cross the Fermi level E_F in the case of Ir_3Te_8 as shown in Fig. 5. The band structure of Ir_3Te_8 contrasts that of Ir_3Se_8 where only one band crosses E_F .¹⁵ The calculations with or without the SOIs do not seem to yield a noticeable difference in the band structure, chiefly because the states near E_F consist of Ir- e_g or d_z^2 orbitals rather than Ir- t_{2g} orbitals (for which the SOI is a first-order effect).

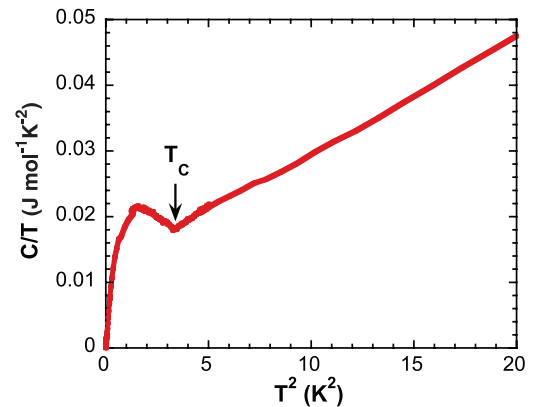


FIG. 4. (Color online) The specific heat $C(T)$ divided by temperature $C(T)/T$ as a function of T^2 for $50 \text{ mK} \leq T \leq 10 \text{ K}$.

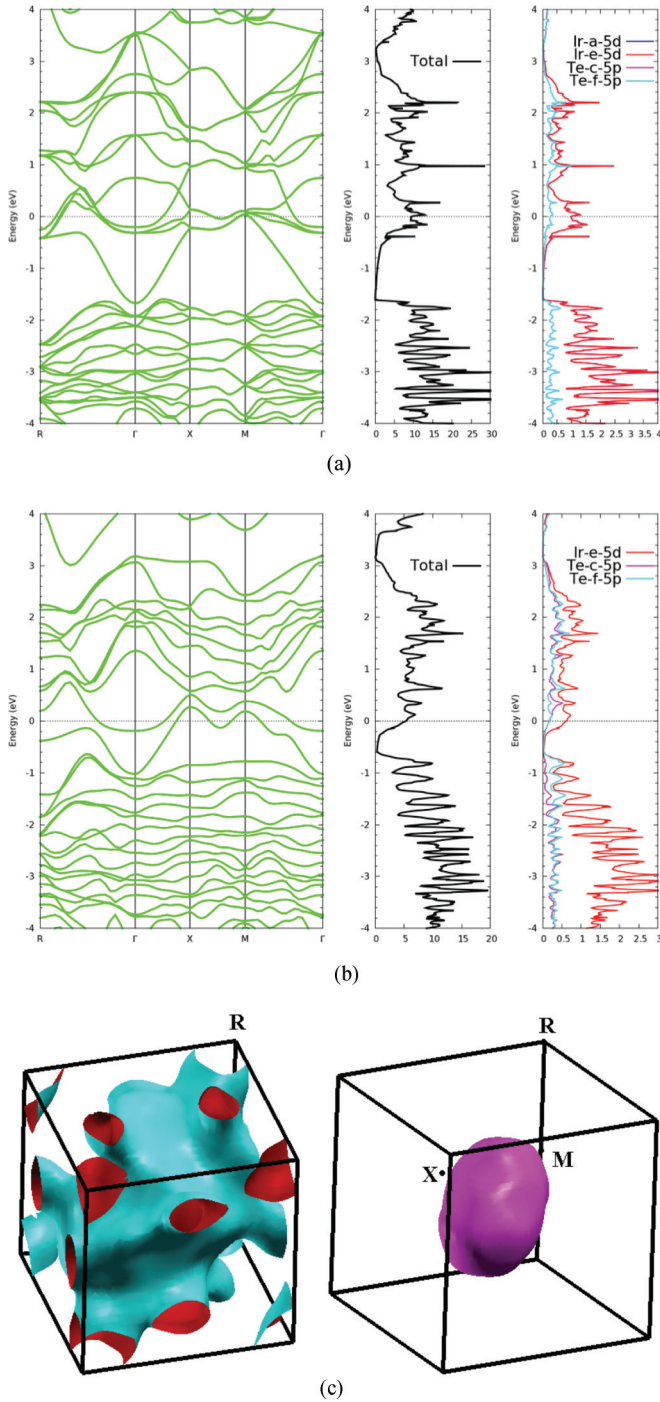


FIG. 5. (Color online) The band structures and density of states (DOS) of (a) Ir_4Te_8 , (b) Ir_3Te_8 , and (c) Fermi surfaces for Ir_3Te_8 : the lower band (left) and the higher band (right). Γ is the center of the Brillouin zone, R (0.5,0.5,0.5), X (0,0.5,0), and M (0.5,0.5,0). The total DOS and momentum-projected DOS are shown in the middle panel and right panel in (a) and (b), respectively. The middle letters are the Wyckoff positions; for instance, “Ir- e -5d” represents the 5d orbital-projected DOS of Ir at positions e .

At $T > T_S = 350$ K, the electronic structure near the Fermi surface is formed primarily by (a) the σ^* anti-bonding state of two Te atoms at the center of the cubic unit cell, and (2) one symmetrized state formed from the

d_z^2 orbitals of the three Ir atoms at positions $(1/2, 1/2, 0)$, $(0, 1/2, 1/2)$, and $(1/2, 0, 1/2)$, which results in a band having strong energy dispersion along the $[111]$ direction. At $T < T_S$, the rhombohedral phase is characterized by two distinct Wyckoff positions a and e in space group $R\bar{3}$; the d_z^2 orbitals of the three Ir ions at position e form a band with some quasi-two-dimensional characteristics. Following a general Landau-Ginzburg symmetry argument, any perturbation of the electronic structure (e.g., via even a weak electron-phonon coupling) in Ir_3Te_8 must lead to a lattice symmetry breaking, which explains the structural transition at $T_S = 350$ K. When an external magnetic field is applied along the $[111]$ direction, a diamagnetic current loop is induced to flow between the three Ir atoms coupled via the symmetrized state of the d_z^2 orbitals. Moreover, the expected diamagnetism must be anisotropic, and the diamagnetic response along $[111]$ should be stronger than that along other directions, which is also consistent with the data shown in Fig. 2(b). This could be an alternative explanation for the anisotropic diamagnetism.

There is an important difference between Ir telluride and the iridates. The oxygen atoms in the iridates carry two additional electrons to complete their p shells. The crystalline-field splitting of the Ir ions is then essentially given by a point-charge model. In sixfold coordination, this yields the t_{2g} orbitals below the e_g states. The t_{2g} orbitals have substantial spin-orbit coupling (e.g., in first-order perturbation), and hence, the physics of the iridates is spin-orbit driven. On the other hand, the Te orbitals participate in covalent bonding. The bonds are directed in the x , y , and z directions of the octahedra. Hence, the energy of the Ir e_g orbitals is lowered more than the energy of the t_{2g} states. Hence, the crystalline electric-field scheme is reverted with respect to the iridates. The e_g orbitals are much less susceptible to the SOI than the t_{2g} states, and hence, Ir_3Te_8 is not driven by the SOI.

V. SUMMARY

All results of Ir_3Te_8 presented here indicate an occurrence of bulk superconductivity below $T_C = 1.8$ K; the superconductivity is accompanied by diamagnetism and unsaturated resistivity that persist over an unusually wide temperature interval of $20 \text{ K} < T < 700 \text{ K}$, spanning a structural transition at $T_S = 350$ K, through which the resistivity slope remains unchanged. The observed lattice transition could be attributed to quasi-two-dimensional properties of a band crossing at the Fermi level. However, the relationship of the superconducting state below $T_C = 1.8$ K to the structural phase transition, the unusual normal state, and the incomplete occupation of the Ir sites in Ir_3Te_8 poses a challenge to our understanding of Ir-based materials.

ACKNOWLEDGMENTS

This work was supported by the NSF through Grants No. DMR-0856234 and No. EPS-0814194; J.H. acknowledges support from the Ministry of Science and Technology of China 973 program (Grant No. 2012CB821400) and Grant No. NSFC-1190024. L.E.D. and P.S. acknowledge the support of the US Department of Energy Grants No. DE-FG02-97ER45653 and No. DE-FG02-98ER45707,

respectively. X.X.W. thanks H. M. Weng for enlightening discussions. We thank N. Dilley at Quantum Design for

measurements of milli-Kelvin heat capacity and electric resistivity.

*Paul Lawrence Dunbar High School, Lexington, Kentucky 40513.

†Corresponding author: cao@uky.edu

- ¹B. J. Kim, H. Jin, S. J. Moon, J.-Y. Kim, B.-G. Park, C. S. Leem, J. Yu, T. W. Noh, C. Kim, S.-J. Oh, J.-H. Park, V. Durairaj, G. Cao, and E. Rotenberg, *Phys. Rev. Lett.* **101**, 076402 (2008).
- ²J. E. Lorenzo, C. Mazzoli, N. Jaouen, C. Detlefs, D. Mannix, S. Grenier, Y. Joly, and C. Marin, *Phys. Rev. Lett.* **101**, 226401 (2008).
- ³B. J. Kim, H. Ohsumi, T. Komesu, S. Sakai, T. Morita, H. Takagi, and T. Arima, *Science* **323**, 1329 (2009).
- ⁴L. Fu, C. L. Kane, and E. J. Mele, *Phys. Rev. Lett.* **98**, 106803 (2007).
- ⁵J. E. Moore and L. Balents, *Phys. Rev. B* **75**, 121306(R) (2007).
- ⁶Y. Xia, D. Qian, D. Hsieh, L. Wray, A. Pal, H. Lin, A. Bansil, D. Grauer, Y. S. Hor, R. J. Cava, and M. Z. Hasan, *Nat. Phys.* **5**, 398 (2009).
- ⁷F. Wang and T. Senthil, *Phys. Rev. Lett.* **106**, 136402 (2011).
- ⁸X. Wan, A. Vishwanath, and S. Y. Savrasov, *Phys. Rev. Lett.* **108**, 146601 (2012).
- ⁹B. J. Yang and Y. B. Kim, *Phys. Rev. B* **82**, 085111 (2010).
- ¹⁰A. Shitade, H. Katsura, J. Kuneš, X.-L. Qi, S.-C. Zhang, and N. Nagaosa, *Phys. Rev. Lett.* **102**, 256403 (2009).
- ¹¹D. A. Pesin and Leon Balents, *Nat. Phys.* **6**, 376 (2010).
- ¹²Y. Zhou, P. A. Lee, T.-K. Ng, and F.-C. Zhang, *Phys. Rev. Lett.* **101**, 197201 (2008).
- ¹³L. Fu and E. Berg, *Phys. Rev. Lett.* **105**, 097001 (2010).
- ¹⁴P. C. Liao, C. H. Ho, Y. S. Huang, and K. K. Tiong, *J. Cryst. Growth* **171**, 586 (1997).
- ¹⁵Y. Qi, S. Matsuishi, J. Guo, H. Mizoguchi, and H. Hosono, *Phys. Rev. Lett.* **109**, 217002 (2012).
- ¹⁶J. J. Yang, Y. J. Choi, Y. S. Oh, A. Hogan, Y. Horibe, K. Kim, B. I. Min, and S.-W. Cheong, *Phys. Rev. Lett.* **108**, 116402 (2012).
- ¹⁷S. Y. Zhou, B. Y. Pan, X. Qiu, J. Pan, X. C. Hong, X. L. Li, Z. Zhang, J. J. Yang, Y. S. Oh, S.-W. Cheong, and S. Y. Li, arXiv:1209.4229.
- ¹⁸A. F. Fang, G. Xu, T. Dong, P. Zheng, and N. L. Wang, *Sci. Rep.* **3**, 1153 (2013).
- ¹⁹D. Ootsuki, S. Pyon, K. Kido, M. Nohara, M. Horio, T. Yoshida, A. Fujimori, M. Arita, H. Anzai, H. Namatame, M. Taniguchi, N. L. Saini, and T. Mizokawa, arXiv:1207.2613.
- ²⁰T. F. Smith, L. E. De Long, A. R. Moodenbaugh, T. H. Geballe, and R. E. Schwall, *J. Phys. C* **5**, L230 (1972).
- ²¹K. Kawabata, *J. Phys. Soc. Jpn.* **54**, 762 (1984).
- ²²E. A. Lynton, *Superconductivity* (Methuen, London, 1969), Chap. 1.
- ²³G. Cao, J. Bolivar, S. McCall, J. E. Crow, and R. P. Guertin, *Phys. Rev. B* **57**, R11039 (1998).
- ²⁴G. Cao, J. E. Crow, R. P. Guertin, P. Henning, C. C. Homes, M. Strongin, D. N. Basov, and E. Lochner, *Solid State Commun.* **113**, 657 (2000).
- ²⁵G. Cao, Y. Xin, C. S. Alexander, J. E. Crow, P. Schlottmann, M. K. Crawford, R. L. Harlow, and W. Marshall, *Phys. Rev. B* **66**, 214412 (2002).
- ²⁶O. B. Korneta, S. Chikara, S. Parkin, L. E. DeLong, P. Schlottmann, and G. Cao, *Phys. Rev. B* **81**, 045101 (2010).
- ²⁷M. Ge, T. F. Qi, O. B. Korneta, D. E. De Long, P. Schlottmann, W. P. Crummett, and G. Cao, *Phys. Rev. B* **84**, 100402(R) (2011).
- ²⁸G. Kresse and J. Hafner, *Phys. Rev. B* **47**, 558 (1993).
- ²⁹G. Kresse and J. Furthmüller, *Comput. Mater. Sci.* **6**, 15 (1996).
- ³⁰G. Kresse and J. Furthmüller, *Phys. Rev. B* **54**, 11169 (1996).
- ³¹J. P. Perdew, K. Burke, and M. Ernzerhof, *Phys. Rev. Lett.* **77**, 3865 (1996).
- ³²D. D. Koelling and B. N. Harmon, *J. Phys. C* **10**, 3107 (1977).
- ³³H. J. Monkhorst and J. Pack, *Phys. Rev. B* **13**, 5188 (1976).
- ³⁴G. M. Sheldrick, *Acta Crystallogr., Sect. A: Found Crystallogr. A* **64**, 112 (2008).
- ³⁵G. M. Sheldrick, *SADABS* (University of Göttingen, Germany, 1996).
- ³⁶E. F. Hocking and J. G. White, *J. Phys. Chem.* **64**, 1042 (1960).
- ³⁷S. Jöbic, M. Evain, R. Brec, P. Debiard, A. Jouanneaux, and J. Rouxel, *J. Solid State Chem.* **95**, 319 (1991).
- ³⁸G. Cao, W. H. Song, Y. P. Sun, and X. N. Lin, *Solid State Commun.* **131**, 331 (2004).
- ³⁹N. F. Mott, *Philos. Mag.* **26**, 1015 (1972).
- ⁴⁰A. F. Ioffe and A. R. Regel, *Prog. Semicond.* **4**, 237 (1960).
- ⁴¹J. H. Mooij, *Phys. Status Solidi A* **17**, 521 (1973).
- ⁴²M. Weger and N. F. Mott, *J. Phys. C* **18**, L201 (1985).
- ⁴³M. B. Maple and K.-S. Kim, *Phys. Rev. Lett.* **23**, 118 (1969).